Mimicking and Understanding the Agglutination Effect of the Antimicrobial Peptide Thanatin Using Model Phospholipid Vesicles

ARTICLE *in* BIOCHEMISTRY · JUNE 2015

Impact Factor: 3.02 · DOI: 10.1021/acs.biochem.5b00442 · Source: PubMed

6 AUTHORS, INCLUDING:

Emile Robert

Laval University

3 PUBLICATIONS **1** CITATION

SEE PROFILE

Thierry Lefèvre

Laval University

54 PUBLICATIONS **1,181** CITATIONS

SEE PROFILE

Matthieu Fillion

Laval University

7 PUBLICATIONS **10** CITATIONS

SEE PROFILE

Michèle Auger

Laval University

144 PUBLICATIONS **4,377** CITATIONS

SEE PROFILE

BIOCHEMISTRY
including biophysical chemistry & molecular biology

Article

pubs.acs.org/biochemistry

Mimicking and Understanding the Agglutination Effect of the Antimicrobial Peptide Thanatin Using Model Phospholipid Vesicles

Émile Robert, Thierry Lefèvre, Matthieu Fillion, Benjamin Martial, Justine Dionne, and Michèle Auger*

Department of Chemistry, Regroupement québécois de recherche sur la fonction, la structure et l'ingénierie des protéines (PROTEO), Centre de recherche sur les matériaux avancés (CERMA), Centre québécois sur les matériaux fonctionnels (CQMF), Université Laval, Québec, QC, Canada G1V 0A6

Supporting Information

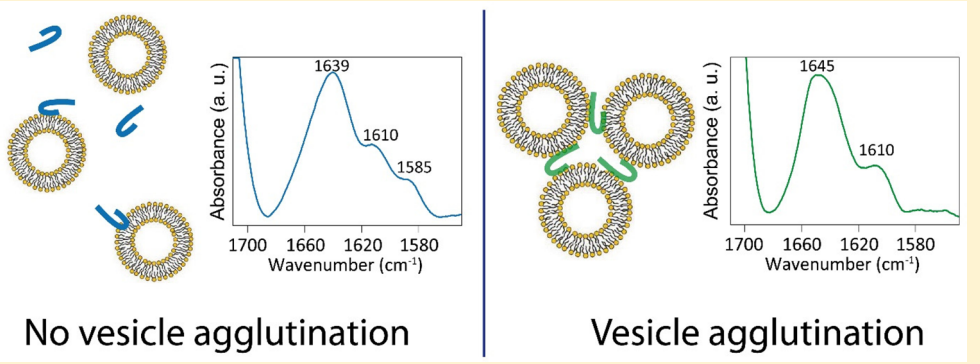

ABSTRACT: Thanatin is a cationic 21-residue antimicrobial and antifongical peptide found in the spined soldier bug *Podisus maculiventris*. It is believed that it does not permeabilize membranes but rather induces the agglutination of bacteria and inhibits cellular respiration. To clarify its mode of action, lipid vesicle organization and aggregation propensity as well as peptide secondary structure have been studied using different membrane models. Dynamic light scattering and turbidimetry results show that specific mixtures of negatively charged and zwitterionic phospholipid vesicles are able to mimic the agglutination effect of thanatin observed on Gram-negative and Gram-positive bacterial cells, while monoconstituent ("conventional") models cannot reproduce this phenomenon. The model of eukaryotic cell reveals no particular interaction with thanatin, which is consistent with the literature. Infrared spectroscopy shows that under the conditions under which vesicle agglutination occurs, thanatin exhibits a particular spectral pattern in the amide I′ region and in the region associated with Arg side chains. The data suggest that thanatin mainly retains its hairpin structure, Arg residues being involved in strong interactions with anionic groups of phospholipids. In the absence of vesicle agglutination, the peptide conformation and Arg side-chain environment are similar to those observed in solution. The data show that a negatively charged membrane is required for thanatin to be active, but this condition is insufficient. The activity of thanatin seems to be modulated by the charge surface density of membranes and thanatin concentration.

Antimicrobial resistance is a natural phenomenon that is amplified by antibiotic misuse in medicine and the food industry.[1] It represents a serious public health threat, especially in the hospital environment where it is the cause of many infections. Currently, the arsenal of available antibiotics is becoming less effective for the treatment of infections involving multiresistant strains of bacteria such as methicillin-resistant *Staphylococcus aureus* and vancomycin-resistant *Enterococcus*.[2,3] The number of new antibacterial agents approved by the U.S. Food and Drug Administration (FDA) is continuously decreasing mainly because of economic considerations,[4] and also because very few novel classes of antibiotics have been developed in the past 30 years.[5] Therefore, the development of new and efficient antibiotics is needed to save lives and to leave time for societies to reexamine and transform their animal husbandry and healthcare strategies.[1]

Among promising new alternatives, antimicrobial peptides (AMPs) are recognized to be part of the next generation of tools available to fight infectious diseases.[6] Remarkable examples of such peptides have initially been found in nature as they constitute a key component in the innate immune system of various species, from lower to higher organisms such as bacteria and mammals.[7] Their presence throughout all life forms suggests an ancient origin. Despite their diversity, AMPs tend to share common characteristics such as a short length (20−50 amino acids), a net positive charge, and a marked amphiphilic character.[8] They are generally active against a broad range of pathogens, including bacteria [both Gram-

Received: April 23, 2015
Revised: June 8, 2015

DOI: 10.1021/acs.biochem.5b00442
Biochemistry XXXX, XXX, XXX−XXX

positive (G+) and Gram-negative (G−)], viruses, and fungi, sometimes regardless of whether the strain developed resistance to conventional antibiotics.[7,9−12] In contrast to standard human-made antibiotics, they usually do not act by altering specific metabolic pathways. They instead target the cellular membrane of bacteria where they induce defects that will eventually cause an electrochemical gradient leading to cell death.[13−15] Thereby, the acquisition by bacteria of mechanisms of resistance toward these molecules is less likely to occur.

Thanatin, an AMP found in the spined soldier bug *Podisus maculiventris*, exhibits a broad spectrum of activity against G+ and G− bacteria and fungi.[16] By contrast, thanatin does not seem to interact with eukaryotic cells. In particular, it has been shown not to be hemolytic.[16] Moreover, the cytoplasmic membrane is not the target of thanatin, and it seems to have a different mode of action, or maybe several.[16] This 21-residue peptide (GSKKPVPIIYCNRRTGKCQRM) indeed does not disorder or permeabilize the bacterial cell membrane, as the cytoplasmic K^+ content is not influenced by the presence of thanatin.[16] It rather blocks the motility of cells and induces their agglutination (in the following, agglutination and aggregation will be used indiscriminately).[16] Lipopolysaccharides (LPS) have been suggested to be responsible for the binding of thanatin to the cell surface of G− bacteria.[16]

From a structural viewpoint, this peptide shares sequence similarities with other AMP families such as brevinins, protegrins, and tachyplesins.[17] Its structure in solution consists of a C-terminal β-hairpin, i.e., a two-stranded β-sheet connected by a cationic loop and stabilized by one disulfide bridge between Cys11 and Cys18, with a structurally variable seven-residue N-terminal region.[17] Some results suggest that thanatin activity against G− bacteria specifically involves arginine 20 (Arg20) which is embedded in a hydrophobic environment.[16,17] The salt concentration seems also to modulate the activity of thanatin as its minimal inhibitory concentration (MIC) increases with an increasing NaCl concentration.

Despite remarkable advances, the mechanism of action of this peptide remains unclear, and a better understanding of its influence on phospholipid vesicles is required. To this end, the interactions between thanatin and phospholipid membranes have been investigated in this study using specific bilayer models, including conventional, monoconstituent saturated-chain phospholipid membranes and binary lipid mixture systems. The size distribution, turbidimetry, and stability of the colloidal lipid suspensions have been followed using dynamic light scattering (DLS) and UV−vis spectroscopy. It appears that the choice of the model is crucial for adequately mimicking the agglutination effect of thanatin. Suitable vesicles can then be used to adequately investigate the biological effect of thanatin on cell membranes. The secondary structure of the peptide has also been assessed using infrared (IR) transmission spectroscopy and electronic circular dichroism (ECD), whereas lipid organization has been investigated by IR and nuclear magnetic resonance (NMR) spectroscopies. It is found that when thanatin induces the agglutination of phospholipid vesicles, it displays a specific spectrum (i.e., different from that obtained in solution). Analysis of these spectra in conjunction with ECD data suggests that thanatin remains in a β-hairpin form and that Arg residues may be involved in strong interactions with anionic groups, probably the phosphate moiety of lipid polar headgroups.

MATERIALS AND METHODS

Materials. All membrane constituents, including phospholipids {dimyristoylphosphatidylcholine (DMPC), dimyristoylphosphatidylglycerol (DMPG), 1-palmitoyl-2-oleoyl-*sn*-glycero-3-phosphocholine (POPC), 1-palmitoyl-2-oleoyl-*sn*-glycero-3-phosphoethanolamine (POPE), 1-palmitoyl-2-oleoyl-*sn*-glycero-3-phosphoglycerol (POPG), and 1′,3′-bis(1,2-dioleoyl-*sn*-glycero-3-phospho)-*sn*-glycerol [tetraoleoylcardiolipin (TOCL)]} and cholesterol, were purchased from Avanti Polar Lipids (Alabaster, AL) and used without further purification. 2,2,2-Trifluoroethanol (TFE), deuterated 2,2,2-trifluoroethanol (TFE-d_3), 1,2-ethanedithiol (EDT), ethylenediaminetetraacetic acid disodium (EDTA), HCl, 4-(2-hydroxyethyl)-1-piperazineethanesulfonic acid (HEPES), and NaCl were purchased from Sigma-Aldrich (St. Louis, MO). Deuterium oxide (D_2O) was obtained from CDN isotopes (Pointe-Claire, QC). Water used for buffer preparation was distilled and deionized using a Barnstead (Boston, MA) NANOpurII system (resistivity of 18.2 MΩ/cm) with four purification columns. All solvents were of reagent grade or HPLC grade quality, purchased commercially, and used without any further purification. Fmoc-protected amino acids, Wang resin, and other solid phase peptide synthesis-related reagents were purchased from Matrix Innovation (Québec, QC). All other chemicals were of reagent grade.

Peptide Synthesis. Thanatin was synthesized using the solid phase peptide synthesis technique by sequentially adding N-Fmoc-protected amino acids to the chain, fixed on Wang resin (substitution of 0.46 mmol/g), as previously described.[18] When the peptide was cleaved from the resin, 2.5% 1,2-ethanedithiol (EDT) was added in a trifluoroacetic acid (TFA) solution to prevent oxidation of the methionine residue. The intramolecular disulfide bridge was formed by bubbling air in a 0.1 M $(NH_4)HCO_3$ solution containing the peptide, at room temperature for 3 h. Residual TFA salts were removed by repeated dissolution of the peptide in 10 mM HCl followed by lyophilization overnight. After five cycles, the strong IR band at 1672 cm^{-1} associated with the trifluoroacetate ion[19] was no longer visible, indicating that TFA was completely removed. The complete synthesis of thanatin was confirmed by liquid chromatography−mass spectrometry (LC−MS).

Sample Preparation. *Multilamellar Vesicles (MLVs).* All MLV samples for IR and NMR measurements were prepared from commercially available lipid solutions (25 mg/mL in $CHCl_3$/MeOH). They were used either pure or mixed, depending on which membrane model was made. The desired amount of lipids was dried under a stream of nitrogen gas before being freeze-dried overnight to remove any trace of residual solvent. The samples were kept at −20 °C until the day of analysis. Lipid samples were hydrated [80% (w/w) of the total mass] in a 10 mM HEPES buffer solution with 5 mM EDTA (pH 7.4). The buffer for IR spectroscopy was prepared using D_2O to avoid loss of spectral information in the amide I′ region due to the overlap with the water OH deformation band. For thanatin-containing samples, the peptide was dissolved in the buffer solution, before hydration. Every sample was then processed through five cycles of mechanical agitation, freezing in liquid nitrogen, and heating at 50 °C. It was finally frozen one last time and thawed at room temperature.

Large Unilamellar Vesicles (LUVs). To prepare LUV samples for DLS and turbidity measurements, lipids were mixed in a glass vial, then dried, and stored as described for

DOI: 10.1021/acs.biochem.5b00442
Biochemistry XXXX, XXX, XXX−XXX

MLV samples. Lipids were suspended in HEPES buffer at a total concentration of 20 mM and stirred for 1 h. For samples containing 150 mM NaCl, the salt was diluted in the buffer solution at the beginning. The resulting suspension was extruded through a polycarbonate membrane with 100 μm diameter pores (Whatman, Pittsburgh, PA) mounted in a Mini-Extruder (Avanti, Alabaster, AL). After 21 passages through the membrane, the LUV solution was diluted in HEPES buffer to yield a final lipid concentration of 0.1 mg/mL at which analyses were performed. Fresh LUV solutions were used for all experiments.

Spectroscopic Techniques. *Infrared Spectroscopy.* IR spectra were recorded using a Nicolet Magna 560 spectrometer (Thermo Fisher Scientific Inc., Waltham, MA) equipped with a nitrogen-cooled MCT (mercury−cadmium−telluride) A detector. The samples were deposited between two CaF_2 windows forming a sealed cell with a 35 μm path length (BioTools, Wauconda, IL) that was inserted in a regulated temperature holding device. Each measurement is an average of 128 scans recorded at a resolution of 2 cm^{-1} using a Happ−Genzel apodization. All data manipulations were performed with Grams/AI 8.0 software (Galactic Industries, Salem, MA). After subtraction of the reference and buffer spectra, baseline corrections were applied using a cubic function, between 3050 and 2750 cm^{-1} for the methylene stretching $\nu_s(CH_2)$ vibration region and between 1685 and 1550 cm^{-1} for the amide I′ region (amide I′ refers to the fact that spectra were recorded in D_2O). Second-derivative spectra have been calculated using the Savitzky−Golay method[20] using a quadratic deconvolution function and 49-point smoothing.

^{31}P NMR Experiments. Proton-decoupled ^{31}P solid-state NMR spectra were recorded on a Bruker Avance 400 MHz spectrometer (Bruker Biospin, Milton, ON). MLV suspensions were introduced in a 4 mm solid-state NMR tube. Spectra were recorded at 161.9 MHz with a Hahn echo sequence[21] and two-pulse phase modulation (TPPM) proton decoupling.[22] Using 2000 scans and 4096 data points, the spectra were acquired with a pulse length of 4.5 μs and a recycle delay of 4 s. The spectral width was 50 kHz, and a line broadening of 50 Hz was applied to all spectra. The chemical shifts were referenced relative to external 85% H_3PO_4 (0.0 ppm).

Electronic Circular Dichroism (ECD). Analyses were performed using a Jasco J-815 instrument (Jasco Corp., Easton, MD) using freshly prepared aqueous solutions of peptides at a concentration of 0.2 mg/mL (82 μM). Spectra were recorded at 37 °C in quartz cylindrical cells with a 0.1 cm path length. Ten scans were collected from 250 to 190 nm with a data pitch of 0.2 nm and a scanning speed of 50 nm/min. The spectra of the buffers were subtracted from the spectra of the corresponding peptide solutions.

Dynamic Light Scattering (DLS) Measurements. The mean diameter of LUV and aggregates was measured using a Zetasizer Nano ZS instrument (Malvern, U.K.) with a 4 mW He−Ne laser emitting at 633 nm. Scattered light was detected at 173° of the incident beam with an APD detector. The LUV solutions were placed in disposable acrylic cells (1.0 cm path length). Thanatin was introduced via a 10 mg/mL solution in HEPES buffer to yield a final concentration of 100 μM. Measurements were taken 30 min and 4 h after addition of the peptide. Control solutions were measured each time to ensure that LUV suspensions were stable. Samples were stabilized at 37 °C for 300 s before each measurement.

Turbidity Experiments. LUV agglutination results in an increase in the turbidity of the solution. Turbidity was then monitored on the basis of the absorbance at 450 nm using a Cary 500 (Varian, Palo Alto, CA) double-beam spectrophotometer equipped with a tungsten lamp and a PMT detector. The choice of the measurement frequency is based on the fact that no contribution of the lipids arises at 450 nm.[23] The LUV solutions were placed in disposable acrylic cells (1.0 cm path length). Thanatin was introduced at various final concentrations via the same HEPES solution described before. Samples were gently shaken between each data point to restore homogeneity and to prevent loss of absorbance caused by sedimentation.

RESULTS AND DISCUSSION

The impact of thanatin on phospholipid vesicles has been evaluated using various phospholipid mixtures. In a first step, as commonly assumed,[24] simple membranes made of pure DMPC or DMPG have been used to mimic eukaryotic and bacterial cells, respectively. These simple models will hereafter be termed conventional models. Considering the membrane composition of both G− and G+ bacteria as well as eukaryotic cells, these conventional models may be too simplistic to adequately mimic the interactions between peptides and real membranes. In general, G− and G+ bacteria contain a considerable amount of zwitterionic phosphatidylethanolamine (PE) combined with anionic phospholipids such as phosphatidylglycerol (PG) and cardiolipins.[10,25,26] For G− bacteria, they contain a larger amount of PE and the most abundant anionic phospholipid is PG.[10,25,26] Some G+ bacteria may contain a significant amount of PE, but this phospholipid can also be totally absent in others. Membranes of G+ bacteria also include a large amount of anionic phospholipids, especially cardiolipin and PG.[10,25,26] For mammalian cells, the outer membrane leaflet contains zwitterionic phosphatidylcholine (PC) and sphingomyelin whereas the inner leaflet contains PE and phosphatidylserine (PS). In addition, cholesterol (30−40%) modulates membrane fluidity.[10,25,26] The membranes of both eukaryotic and bacterial cells contain a large amount of unsaturated-chain lipids. By taking into account all previous statements and the literature, we found Eu, G+, and G− cells were mimicked with POPC/Chol (8:2 molar ratio), POPG/TOCL (6:4 molar ratio), and POPE/POPG (7:3 molar ratio) mixtures, respectively. The lipid composition of the membrane models is detailed in Table 1.

Molecular Interactions between Thanatin and Phospholipid Membranes. ^{31}P has a 100% isotopic abundance and a spin of $^1/_2$, which makes this nucleus of great interest for solid-state NMR studies involving phospholipid membranes. It is well-known that the different phases and arrangements adopted by phospholipids can be represented by a specific

Table 1. Lipid Compositions of the Membrane Models Selected

model	lipid	molar proportions
G−	POPE	7
	POPG	3
G+	POPG	6
	TOCL	4
Eu	POPC	8
	Chol	2

DOI: 10.1021/acs.biochem.5b00442
Biochemistry XXXX, XXX, XXX−XXX

shape and width of the powder spectrum.[27,28] The dominant interaction is the chemical shift anisotropy (CSA) and is sensitive to variations in the dynamics and/or orientation of the lipid polar headgroups.

Figure 1 shows the ^{31}P solid-state NMR spectra of phospholipid MLVs in the absence and presence of thanatin

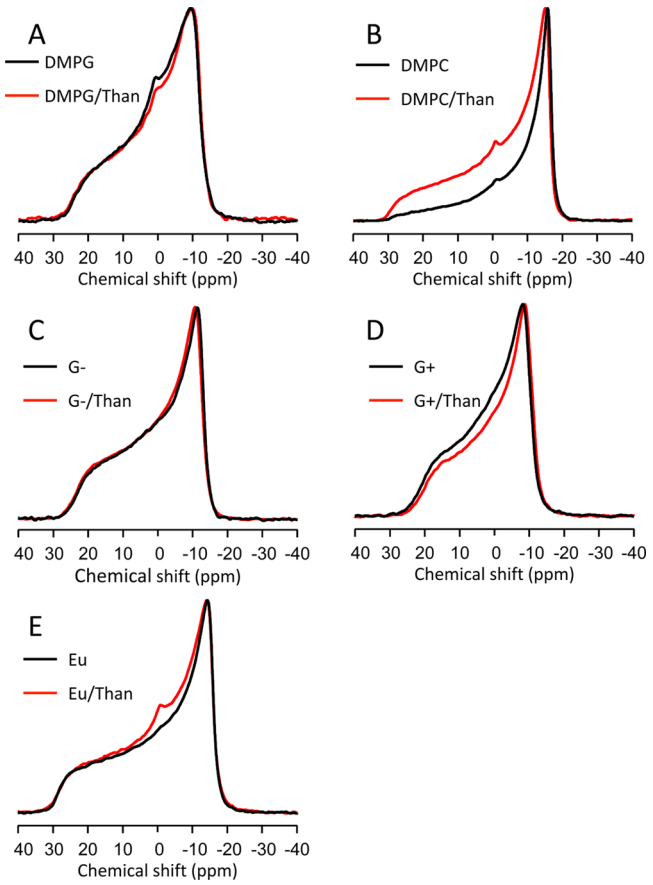

Figure 1. ^{31}P NMR spectra of MLVs composed of (A) DMPG, (B) DMPC, (C) a G− model, (D) a G+ model, and (E) a Eu model, in the absence and presence of thanatin (lipid:thanatin molar ratio of 60:1).

(lipid:thanatin molar ratio of 60:1). There is overall no significant difference in the powder spectrum when thanatin is present as compared to the pure vesicles, regardless of the membrane model used. This observation indicates that thanatin does not (significantly) perturb the vesicle deformability or the local orientation of the lipid polar headgroups, regardless of the model used. However, a small change in the spectral line shape is observed for DMPC vesicles (Figure 1B). This result suggests DMPC MLVs remain more spherical in the magnetic field when thanatin is present, suggesting a slight rigidification of the vesicles,[29] or a change in the local orientation of the lipid polar headgroups in the presence of thanatin.

Among the various membrane models investigated, only pure DMPC and DMPG vesicles exhibit a gel-to-fluid phase transition (so-called main phase transition) in a temperature range that can be investigated by our IR spectroscopy system. The lipid thermotropism of DMPC and DMPG has been followed by monitoring the position of the CH_2 symmetric stretching [$\nu_s(CH_2)$] vibration as a function of temperature (Figure S1 of the Supporting Information). Pure DMPC and DMPG MLVs exhibit a well-known sharp increase in the position of the $\nu_s(CH_2)$ band at 21 °C that is due to the conversion of *trans* to *gauche* C−C bond conformations as a result of the lipid phase transition.[30−32] No significant effect is observed on the $\nu_s(CH_2)$ temperature profile of DMPC bilayers in the presence of thanatin, indicating no specific interactions (Figure S1A of the Supporting Information). A slight increase (∼1 °C) in the main phase transition temperature is observed for DMPG bilayers (Figure S1B of the Supporting Information), which suggests that, because of its positive charge, thanatin is located at the negatively charged membrane surface of DMPG, thus inducing a slight compaction of lipid acyl chains due to charge neutralization. Results similar to those obtained with the $\nu_s(CH_2)$ band are obtained by monitoring the position of the carbonyl stretching vibrations (data not shown), suggesting that the interfacial region of the phospholipid bilayers, like the hydrophobic region, is not affected by thanatin. Therefore, although not ruling out completely membrane perturbation as the mechanism of action of thanatin, NMR and IR results do not seem to support it and are in agreement with prior work.[16]

Effect of Thanatin on Agglutination of Phospholipid Vesicles. *DLS Measurements.* DLS measurements provide an estimation of the size distribution of particles in a colloidal suspension. This technique has been used to monitor the effect of thanatin on the size distribution of LUVs of various lipid compositions (Figure 2). The goal is to create models that mimic the cell agglutination observed on living bacteria and to determine whether phospholipids alone, and which phospholipids, can be targeted by the peptide. In addition, because it has been shown that the presence of salt reduces the efficiency of thanatin,[16] these experiments have been conducted with (150 mM) and without NaCl. It is noteworthy that the polydispersity index (data not shown) was very high in most of the measurements where aggregation occurred. This means that the absolute values for mean diameters have to be considered with caution and that the results should be regarded as global trends rather than actual aggregate sizes.

Control LUV solutions in the absence of thanatin show that the size of the vesicles is ∼100 nm, as expected from the sample preparation, and is constant during the experiments for all model systems, showing that all lipid dispersions are stable in the absence of thanatin. When conventional models are used, no sign of aggregation is measured after the addition of 100 μM thanatin, even after 4 h (data not shown). By contrast, as shown in Figure 2, an important increase in the mean diameter value with G− and G+ models is observed upon addition of 100 μM thanatin, which indicates that large aggregates form over time. After a stabilization period of 4 h, both samples contain aggregates a few thousand nanometers large and the solutions are visually cloudy. Aggregates seem smaller for G+ than for G− LUVs. These results are reminiscent of the agglutination phenomenon observed *in vitro* with G− and G+ cells.[16]

With regard to Eu vesicles, like pure DMPC and DMPG models, they do not seem to be affected by the peptide, which is consistent with the absence of erythrocyte agglutination and hemolytic activity of thanatin.[16] The presence of 150 mM NaCl yields significantly smaller aggregates for G− and G+ models. This result is consistent with the fact that the MIC increases with an increasing NaCl concentration, assuming that the extent of aggregation reflects the activity efficiency of thanatin. Vesicles made with the Eu model are as stable in the presence of NaCl as they are in the absence of NaCl. In conclusion, DLS results overall show that thanatin induces the agglutination of

DOI: 10.1021/acs.biochem.5b00442
Biochemistry XXXX, XXX, XXX−XXX

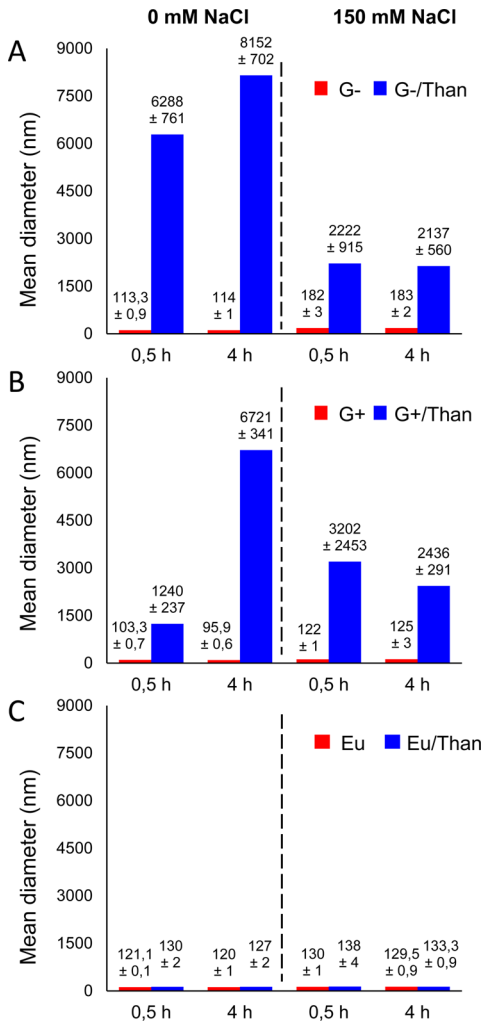

Figure 2. Mean hydrodynamic diameter of LUVs corresponding to (A) G−, (B) G+, and (C) Eu models, in the absence and presence of thanatin, as measured by DLS. Measurements were taken after 30 min or 4 h in the absence and presence of NaCl.

vesicles when the membrane model chosen is appropriate, in concordance with experiments performed on real bacteria, including the effect of salt. It thus seems possible to mimic the biological effect and activity of thanatin on cell model membranes.

Turbidimetry Measurements. Using UV−vis spectrometry for turbidity measurements allows real-time data acquisition for aggregation kinetic analysis, which is impossible to conduct with DLS due to long thermal stabilization periods and acquisition times that take up to several minutes. These experiments are thus complementary with DLS ones. They were conducted with only more complex model systems because conventional ones did not reproduce the biological effect of thanatin.

Figure 3 shows the absorbance at 450 nm as a function of time for G+, G−, and Eu LUVs at different thanatin concentrations. For the G− model, the absorbance rises and remains almost constant at 5 μM thanatin. From 10 to 50 μM, a rapid rise in absorbance occurs, followed by a slower decrease. Visual inspection of the samples shows that in the first stage of the experiment, the solution becomes progressively cloudier. At some point, after the maximal absorbance is reached, large particles become visible to the eye. The suspension is in fact

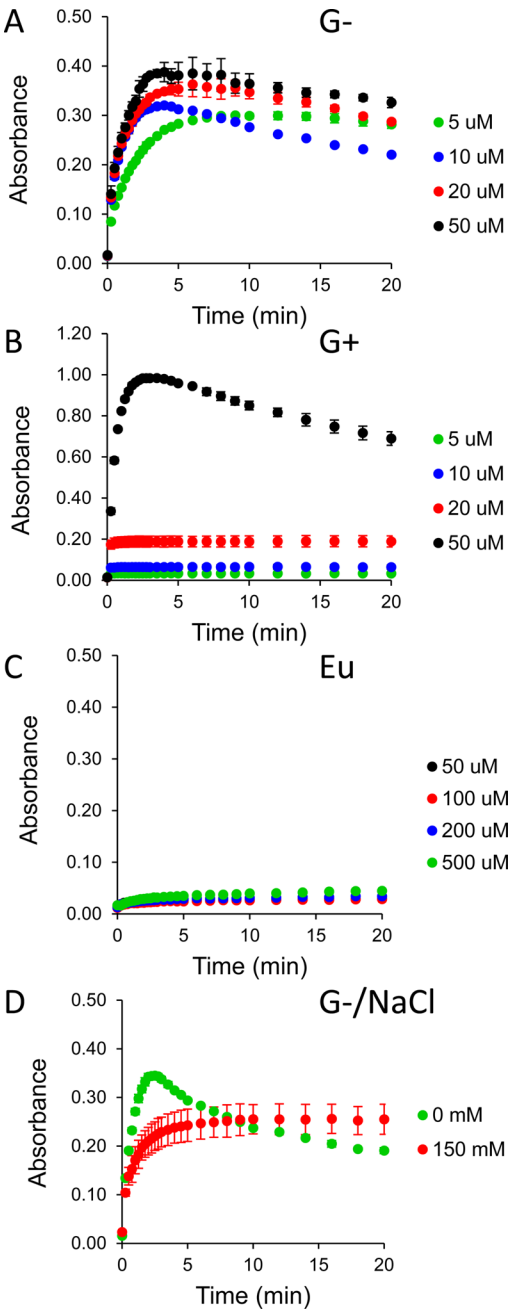

Figure 3. Absorbance at 450 nm as a function of time for LUVs corresponding to (A) G−, (B) G+, and (C) Eu models at different thanatin concentrations. Curve D compares the kinetics of vesicle agglunitation of the G− LUV model in the absence and presence of NaCl with 10 μm thanatin.

composed of white (insoluble) aggregates dispersed in a clear solution (probably due to coacervation), thus allowing more radiation to pass through the sample, which causes the absorbance to decrease. Then, although the absorbance decreases after reaching a maximum, it appears that aggregation actually still continues. For the G+ model (Figure 3B), the absorbance reaches a maximum extremely rapidly at 5, 10, and 20 μM thanatin and then remains stable. The absorbance value at the plateau is lower than that reached for the G− models. The solutions were also visually homogeneous. At 50 μM thanatin, the shape of the curve is similar to that of G− LUVs

DOI: 10.1021/acs.biochem.5b00442
Biochemistry XXXX, XXX, XXX−XXX

(at the lowest concentrations) but the absorbance value attained ($A \sim 1$) is larger than for G− vesicles ($A \sim 0.3$−0.4).

These results indicate that the charge density of the vesicles has an impact on vesicle aggregation. The amplitude of the agglutination phenomenon increases with thanatin concentration, which suggests that thanatin is anchored to the vesicle and reduces the apparent charge of the surface. For thanatin concentrations corresponding to typical MICs (5−20 μM), the agglutination response appears to be more rapid for G+ (100% charged lipids) than for G− (30% charged lipids) LUVs but leads to smaller aggregates. It thus seems that strong electrostatic repulsions between G+ vesicles limit the growth of aggregates, at least for the first 30 min. Another variable is the presence of PE in G− model vesicles that is known to induce a negative curvature in the membrane, which may in turn affect the kinetics of agglutination and the interactions with thanatin.

At a higher thanatin concentration (50 μM), repulsions between vesicles are weakened and the behavior of the G+ model becomes similar to that of the G− model, with the occurrence of insoluble aggregates. Assuming that a higher absorbance at 450 nm indicates larger vesicle aggregates, DLS and turbidimetry data indicate that aggregate size is generally higher for G− bacteria than for G+ bacteria (except at 50 nm), thus suggesting stronger antibacterial activity of thanatin against G− bacteria as compared with G+ bacteria.[33] This therefore suggests that thanatin activity is modulated by the surface charge density of the membrane and peptide concentration.

As a matter of fact, because the charge of the membrane is 30 units per 100 lipids for G− membrane models and 140 units per 100 lipids (each TOCL molecule bears two negative charges) for G+ vesicle models, the charge is ∼5 times higher for G+ than G− vesicles. This would explain why 5 times more thanatin is required to induce the formation of insoluble aggregates for G+ (50 μM thanatin) than for G− (10 μM thanatin) vesicle models.

For the Eu model (Figure 3C), only a slight increase in the absorbance is observed even though higher thanatin concentrations were tested (up to 500 μM), which is consistent with DLS experiments. Finally, the effect of 150 mM NaCl has been studied for the G− model with 10 μM thanatin (Figure 3D). In this case, the absorbance rises to a maximal value and remains stable for the rest of the experiment. Samples were visually homogeneous. The plateau value is lower than the maximal value obtained in the absence of NaCl, which suggests that the extent of vesicle agglutination is lower with NaCl than in the latter case, which is consistent with DLS data and with the lower activity of thanatin at higher ionic strengths. Altogether, these data indicate that electrostatic interactions between thanatin and phospholipids are some of the driving forces for vesicle agglutination.

DLS and turbidimetry data are overall consistent with each other, and both suggest that the extent and kinetics of G− and G+ vesicle agglutination increases with thanatin concentration, although they also depend on the vesicle model used. These conclusions may not be surprising as the thanatin MIC is known to depend on microorganism, even among G− or G+ bacteria themselves.[16] It thus depends in particular on the bacterial membrane composition. It has previously been shown that thanatin presents a strong LPS-binding site, to which could be attributed its anti-Gram-negative activity.[17,34] Current experiments show that thanatin also diplays a great affinity for phospholipids typically found in bacterial lipid bilayers in a way that resembles reported observations of its *in vivo* activity.[16,35] Our G− and G+ models suggest that PG or at least negatively charged lipids are required to make thanatin active against cell membranes. This is not sufficient, however, because pure DMPG LUVs are insensitive to aggregation in the presence of thanatin. Another component, zwitterionic or anionic (PE or cardiolipin), seems also to be necessary.

Structure of Thanatin in an Aqueous Solution. Figure 4 shows the raw (Figure 4A) and second-derivative (Figure 4B)

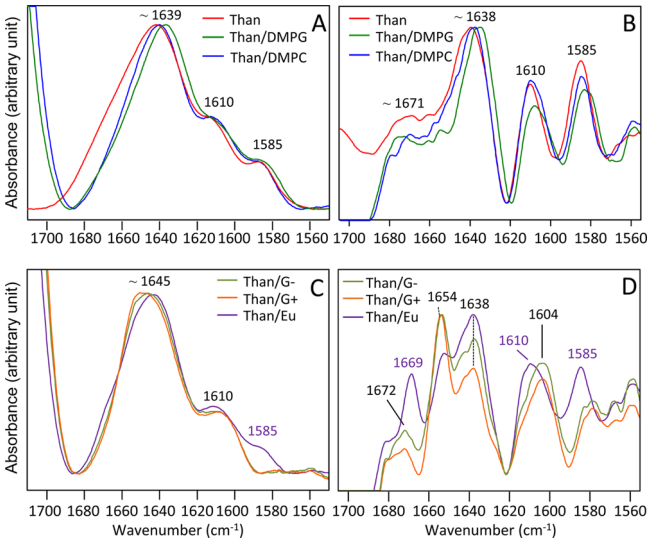

Figure 4. Infrared spectra (A and C) and second-derivative infrared spectra (B and D) at 25 °C in the amide I′ region of (A and B) thanatin in a D_2O solution at pH 7.4 in the presence of DMPC and DMPG MLVs and (C and D) thanatin in the presence of G−, G+, and Eu MLV model membranes. Spectra are normalized with respect to the amide I′ maximum.

IR spectra of thanatin in aqueous solution and in the presence of DMPC and DMPG MLVs, in the amide I′ region (1600−1700 cm^{-1}). This spectral region mostly originates from the carbonyl stretching mode of the peptide bond.[36] The amide I′ band is known to be sensitive to the secondary structure adopted by polypeptide chains[37,38] and has thus been used to evaluate the conformation of thanatin, in particular in the presence of vesicles of various compositions.

In aqueous solution, the amide I′ band of thanatin is characterized by a maximum at 1641 cm^{-1}. It is broad with an asymmetric shape, showing a certain heterogenity of the secondary structure. The position of the peak maximum value lies between what would be expected for a structure principally composed of random coil (1645−1650 cm^{-1}) and that of β-sheet (1630−1635 cm^{-1}).[39,40] The spectrum is quite broad, suggesting that other, less defined secondary structural elements are also present. The second derivative shows a main component at 1640 cm^{-1} assigned to a loose β-sheet, accompanied by a broad multicomponent feature centered at ∼1671 cm^{-1} attributed to turns and disordered structures[40] that probably originate from the N-terminal region of the peptide. The IR spectrum and its interpretation are in agreement with the three-dimensional hairpin structure of thanatin as determined from NMR.[17] It is in fact similar to spectra obtained with other β-hairpin peptides.[41−43] Small bands located at 1610 and 1585 cm^{-1} are due to the antisymmetric $[\nu_{as}(CN_3H_5^+)]$ and symmetric $[\nu_s(CN_3H_5^+)]$ N−H stretching

DOI: 10.1021/acs.biochem.5b00442
Biochemistry XXXX, XXX, XXX−XXX

vibration of the guadinino group of arginine (Arg), respectively.[36,44,45] The position of these bands has been found to be sensitive to protonation, ion pairing, and the environment in which it occurs.[45] These bands are representative of the three Arg residues that thanatin contains, and they may be a probe for Arg environment.

ECD has been used as a complementary structural investigation technique. The spectrum of thanatin in aqueous solution (Figure S2A of the Supporting Information) is characterized by a minimum near 200 nm. The spectrum is identical in HEPES, Tris, or phosphate buffer and is concentration-independent in the concentration range of 0.05−1.00 mg/mL (data not shown). This spectrum is in agreement with that previously reported.[33] Such a spectrum does not correspond to any known pure secondary structure (it is broader than that of random coil), but the literature shows that it is representative of other β-hairpin peptides.[46,47] It certainly represents the superposition of contributions from β-sheets, turns, and random coils. An estimation of the secondary structure content as determined from the ECD spectrum using the method developed by the group of Goormaghtigh[48] indeed suggests that thanatin in solution is composed of 35% β-sheets, 41% random coils, 13% turns, and 11% unordered structures.

Structure of Thanatin in the Presence of Conventional Vesicle Models. In Figure 4A, the IR spectrum of thanatin in solution is compared with those recorded in the presence of DMPC or DMPG MLVs. In the presence of these lipid vesicles, the shape of the amide I′ band is basically retained, although it is narrower on the high-frequency side than in solution, which indicates that the secondary structure is slightly more homogeneous in the presence of membranes, most probably because of a decrease in the amount of disordered structures and/or turns. The maximum of the amide I′ band is also slightly shifted toward lower wavenumbers (1640 and 1636 cm^{-1} for DMPG and DMPC, respectively), which is confirmed by the shift in the position of the maximum of the β-sheet component in the second derivatives (1638 and 1636 cm^{-1} for DMPG and DMPC, respectively). These shifts suggest that the hairpin β-sheet is slightly affected by the presence of the membranes. The second derivatives (Figure 4B) show that the spectral pattern of thanatin in the presence of DMPC and DMPG is basically the same as in solution, indicating that the structural modifications of thanatin remain moderate in the presence of conventional model MLVs.

Structure of Thanatin in the Presence of More Realistic Vesicle Models. A completely different spectral pattern is observed for thanatin in the presence of MLVs formed with G− and G+ models (Figure 4C,D), which suggests that the peptide adopts a specific conformation. It is remarkable that the vesicle models that are able to reproduce thanatin-induced agglutination of cells are associated with a particular secondary structure of the peptide. The spectral change is mainly due to a shift of the maximum of the amide I′ band toward a higher wavenumber value (~1645 cm^{-1}) and a flattening of the top of the band. These spectral changes are in fact due to the presence of an additional sharp band at 1654 cm^{-1} as shown by the second-derivative spectra (Figure 4D). This band would be traditionnaly assigned to α-helix structural elements, although an alternative explanation is possible as discussed below. The β-sheet component is still present at 1638 cm^{-1}, suggesting that the β-hairpin remains in these circumstances. Like the spectra obtained in the presence of DMPC and DMPG, a decrease in intensity is observed in the broad 1670 cm^{-1} region, probably due to a loss of turns or disordered structures.

Although similar to those obtained in the presence of G− and G+ models, the amide I′ band obtained in the presence of Eu MLVs differs. It seems also to share some similarities with the spectra of Figure 4A and then seems to be intermediate between G−/G+ and conventional models. The amide I′ band maximum is located at 1642 cm^{-1} due to the lower intensity of the band at 1654 cm^{-1} (Figure 4D). The amide I′ band also exhibits a weak shoulder on its high-frequency side (Figure 4C) that arises from the presence of a sharp band at 1669 cm^{-1} (Figure 4D). This component seems absent or weak for G− and G+ MLVs and likely reveals the presence of turns.

Thanatin also shows a decrease in the intensity of the side-chain vibrations in the presence of G−, G+, and Eu models (Figure 4C), as compared to that of the pure peptide in solution (Figure 4A). In particular, the band at 1585 cm^{-1} completely disappears for G− and G+ membranes. Thus, the specific conformation of thanatin that is related to vesicle agglutination is also associated with a perturbation of the Arg residues. This observation can be associated with the fact that Arg20 is essential for the activity of thanatin.[16]

For the purpose of comparison, the spectra of thanatin have also been observed in the presence of pure POPG vesicles (Figure S3A,B of the Supporting Information). As can be seen, the spectra and their second derivatives are very similar to those of pure DMPG vesicles, suggesting no effect of the *cis* double bond on the interactions between thanatin and PG bilayers. Comparison with G− and G+ membrane models shows, strikingly, that pure POPG bilayers are unable to mimic the biological effect of thanatin. A mixture of POPG with another lipid (PE or cardiolipin) seems necessary, an effect that remains unclear and to be further investigated.

Interpretation of the IR Spectra of Thanatin in the Presence of G−/G+ Model Membranes. Thanatin exhibits three types of spectral patterns in the amide I′ region depending on the type of model membranes. In the presence of DMPC, DMPG, and POPG MLVs, the amide I′ band is close to that of thanatin in solution and is characterized by a predominant β-sheet component and several bands assigned to turns and disordered structures. In the presence of G− and G+ membranes, thanatin is characterized by a decrease in the percentage of turns and disordered structural elements, and the marked presence of the component at 1654 cm^{-1}. This particular spectral signature is accompanied by the disappearance of the component at 1585 cm^{-1} due to Arg side chains. The conformation in the presence of POPC and POPC/cholesterol (Eu) membrane models is intermediate between these two types of spectral features.

The band component at 1654 cm^{-1} may have two assignments. The classical interpretation would lead one to conclude that this component originates from α-helical structural elements. Another possibility is that the Arg band that disappears at 1585 cm^{-1} is shifted to 1654 cm^{-1}. To evaluate the "α-helix hypothesis", thanatin has been dissolved in TFE-d_3/D_2O mixtures to promote the formation of α-helix. The ECD spectrum of thanatin in a TFE/H_2O mixture [98:2 (v/v)] is shown in Figure S2A of the Supporting Information. The general shape is conserved; however, the minimum of the spectrum is now located at 203 nm (instead of 200 nm in H_2O), and the spectrum broadens on the high-frequency side. To determine which secondary structure is responsible for this spectral change, the spectrum of thanatin in H_2O has been

DOI: 10.1021/acs.biochem.5b00442
Biochemistry XXXX, XXX, XXX−XXX

subtracted from the spectrum obtained in the TFE/H_2O mixture. The rationale is that thanatin in a TFE/H_2O mixture may be represented by a superposition of the "native" β-hairpin peptide with other secondary structural elements, assuming that the disulfide bond imposes the persistence of the β-hairpin without overly strong distortions from the native form. Using an appropriate subtraction factor (0.34), one obtains the spectrum in Figure S2B of the Supporting Information, which strikingly resembles the spectrum of an α-helical peptide. Comparison with the spectrum of myoglobin, a model of α-helix protein, supports this finding. Therefore, the spectrum obtained in a TFE/H_2O mixture seems to be the superposition of the native β-hairpin found in solution with α-helical elements.

Similar IR spectra of thanatin in a TFE/D_2O mixture have been obtained (Figure S4A of the Supporting Information) and the second derivatives calculated (Figure S4B of the Supporting Information). Compared with the spectrum in D_2O, the general shape of the amide I′ band is not affected by TFE, although it is shifted toward higher wavenumbers, the maximum of the amide I′ band being located at 1648 cm^{-1} as compared to 1641 cm^{-1} in D_2O. This wavenumber value is commonly associated with α-helix. Thus, both ECD and IR spectra indicate that thanatin forms α-helix in TFE. This seems consistent with the helix propensity of thanatin in the presence of SDS[33] and the helix propensity of brevinin in a membrane-mimetic environment.[49]

However, the general shape of the amide I′ band and the pattern of the second derivatives in a TFE/D_2O mixture do not correspond to what is observed in the presence of G− and G+ membrane models, in particular without a sharp component near 1654 cm^{-1}, suggesting that the conformation is different and that this band is not necessarily due to α-helical segments. In particular, the 1585 cm^{-1} band due to Arg is still present in a TFE/D_2O mixture while it totally disappears with G− and G+ vesicles and should absorb elsewhere. Because Arg amino acids represent 14% of the peptide, their potential contribution in the amide I′ region may not be negligible. Therefore, the 1585 cm^{-1} component of Arg may possibly be shifted to 1654 cm^{-1}. In fact, as shown in a study specifically dedicated to the effect of the type of counterion and solvent on Arg vibrations, $\nu(CN_3H_5^+)$, Arg bands can shift strongly depending on the conditions. Shifts of up to ~40 cm^{-1} are expected when Arg side chains are involved in specific interactions, namely ion pairing, in a hydrophobic environment.[45]

Therefore, the band at 1585 cm^{-1} may be shifted to 1654 cm^{-1} upon strong interactions of the Arg guanidino group with negatively charged groups. A very similar band at 1695 cm^{-1} has indeed been observed in H_2O for halorhodopsin and has been suggested to result from a H-bond between Arg side chains and carboxylate anions (borne by aspartate or glutamate amino acids).[45] Following this interpretation, it may be suggested that Arg side chains of thanatin are involved in a hydrogen bond with the phosphate groups of POPG (or TOCL) in G− and G+ model membranes, although other types of binding such as electrostatic interactions may be put forward. This modification of Arg vibration seems consistent with the fact that Arg20 has been found to be essential for the activity of thanatin.[16,17] Moreover, if the band at 1654 cm^{-1} is actually due to Arg side chains, this implies that the specific spectral pattern observed in the amide I′ region is not due to a conformational change, suggesting that thanatin mainly retains its β-hairpin structure in the case in which vesicle agglutination occurs.

These results are generally consistent with a model previously proposed[35] in which thanatin is located at the membrane surface and induces the agglutination of phospholipid vesicles. These results, however, show that binding of thanatin to vesicles is associated with a particular IR spectral pattern that in fact reflects specific interactions of Arg residues, probably with membranes. Such a change is not observed with DMPG or POPG, showing that particular membrane compositions are required to induce interactions between thanatin and membranes and cause their agglutination. The determinants that are essential to drive vesicle agglunitation and the specific molecular interactions of "active" (membrane-bonded) thanatin remain to be determined.

CONCLUSION

This study shows that with the right combination of phospholipids and bacterial membrane constituents, it is possible to reproduce the agglutination induced by thanatin in ways that resemble previously published *in vivo* results. With adequate models, it is possible to mimic thanatin's selectivity toward bacterial cells, as well as the effect of salt. G− and G+ models seem appropriately mimicked by phospholipid mixture vesicles containing 30 and 100% anionic lipids, respectively. These models could further be used in the future to efficiently investigate the impact of thanatin on cell membranes and better understand its mechanism of action. This study also suggests that Arg residues of thanatin may be involved in strong interactions with anionic groups when vesicles are agglutinated and that anionic lipids are required for interactions to occur, although their mere presence is insufficient to trigger agglutination. Several questions regarding the molecular interactions between thanatin and membranes remain to be elucidated.

ASSOCIATED CONTENT

Supporting Information

Position of the $\nu_s(CH_2)$ of DMPC and DMPG bilayers as a function of temperature in the absence and presence of thanatin (lipid:thanatin molar ratio of 60:1) (Figure S1), ECD spectra of thanatin in H_2O and in a TFE/H_2O (98:2) mixture and subtraction of the spectra using a subtraction factor of 0.34 compared with the typical spectrum of an α-helical protein (myoglobin) (Figure S2), IR spectra and second derivatives of thanatin in the amide I′ region in the presence of POPG vesicles as compared with DMPG, G−, and G+ vesicle models (Figure S3), and IR spectra and second derivatives of thanatin in D_2O and in a TFE/D_2O (75:25) mixture in the amide I′ region (Figure S4). The Supporting Information is available free of charge on the ACS Publications website at DOI: 10.1021/acs.biochem.5b00442.

AUTHOR INFORMATION

Corresponding Author

*Department of Chemistry, PROTEO, CERMA, CQMF, Université Laval, Québec, Québec, Canada G1V 0A6. E-mail: michele.auger@chm.ulaval.ca. Telephone: (418) 656-3393. Fax: (418) 656-7916.

Funding

This work was supported by the Natural Sciences and Engineering Research Council of Canada (NSERC), the Fonds de recherche du Québec-Nature et Technologies (FRQ-NT), the Regroupement québécois de recherche sur la

DOI: 10.1021/acs.biochem.5b00442
Biochemistry XXXX, XXX, XXX−XXX

fonction, la structure et l'ingénierie des protéines (PROTEO), the Centre de recherche sur les matériaux avancés (CERMA), and the Centre québécois sur les matériaux fonctionnels (CQMF). E.R. acknowledges a graduate scholarship from PROTEO.

Notes

The authors declare no competing financial interest.

■ ACKNOWLEDGMENTS

We thank Pierre Audet, Jean-François Rioux-Dubé, and François Paquet-Mercier for their technical assistance with the solid-state NMR and infrared spectroscopy measurements. We also thank François Otis and Pr. Normand Voyer for their assistance in peptide synthesis. Finally, we thank an anonymous reviewer for having made several relevant suggestions, in particular regarding the impact of the membrane charge of bacteria on interactions with thanatin.

■ ABBREVIATIONS

AMP, antimicrobial peptide; CaF_2, calcium fluoride; CSA, chemical shift anisotropy; DLS, dynamic light scattering; DMPC, dimyristoylphosphatidylcholine; DMPG, dimyristoylphosphatidylglycerol; ECD, electronic circular dichroism; EDT, 1,2-ethanedithiol; EDTA, ethylenediaminetetraacetic acid disodium; Fmoc, fluorenylmethyloxycarbonyl; HEPES, 4-(2-hydroxyethyl)-1-piperazineethanesulfonic acid; HCl, hydrochloric acid; HPLC, high-performance liquid chromatography; IR, infrared; LC−MS, liquid chromatrography−mass spectrometry; LPS, lipopolysaccharides; LUV, large unilamellar vesicle; MCT, mercury−cadmium−telluride; MIC, minimal inhibitory concentration; MLV, multilamellar vesicle; NMR, nuclear magnetic resonance; POPC, 1-palmitoyl-2-oleoyl-*sn*-glycero-3-phosphocholine; POPE, 1-palmitoyl-2-oleoyl-*sn*-glycero-3-phosphoethanolamine; POPG, 1-palmitoyl-2-oleoyl-*sn*-glycero-3-phosphoglycerol; TFA, trifluoroacetic acid; TPPM, two-pulse phase modulation; TOCL, 1′,3′-bis(1,2-dioleoyl-*sn*-glycero-3-phospho)-*sn*-glycerol (tetraoleoylcardiolipin); UV−vis, ultraviolet−visible.

■ REFERENCES

(1) *The evolving threat of antimicrobial resistance: Options for action* (2012) pp 1−120, World Health Organization, Geneva.

(2) Levy, S. B., and Marshall, B. (2004) Antibacterial resistance worldwide: Causes, challenges and responses. *Nat. Med. 10*, S122−S129.

(3) Taubes, G. (2008) The bacteria fight back. *Science 321*, 356−361.

(4) Spellberg, B., Guidos, R., Gilbert, D., Bradley, J., Boucher, H. W., Scheld, W. M., Bartlett, J. G., and Edwards, J., Jr. (2008) The epidemic of antibiotic-resistant infections: A call to action for the medical community from the Infectious Diseases Society of America. *Clin. Infect. Dis. 46*, 155−164.

(5) Hamad, B. (2010) The antibiotics market. *Nat. Rev. Drug Discovery 9*, 675−675.

(6) Fjell, C. D., Hiss, J. A., Hancock, R. E. W., and Schneider, G. (2012) Designing antimicrobial peptides: Form follows function. *Nat. Rev. Drug Discovery 11*, 37−51.

(7) Hancock, R. E., and Chapple, D. S. (1999) Peptide antibiotics. *Antimicrob. Agents Chemother. 43*, 1317−1323.

(8) Hancock, R. E. W., and Lehrer, R. (1998) Cationic peptides: A new source of antibiotics. *Trends Biotechnol. 16*, 82−88.

(9) Andres, E., and Dimarcq, J. L. (2007) Cationic antimicrobial peptides: From innate immunity study to drug development. *Médecine et Maladies Infectieuses 37*, 194−199.

(10) Zasloff, M. (2002) Antimicrobial peptides of multicellular organisms. *Nature 415*, 389−395.

(11) Hou, Z., Lu, J., Fang, C., Zhou, Y., Bai, H., Zhang, X., Xue, X., Chen, Y., and Luo, X. (2011) Underlying mechanism of in vivo and in vitro activity of C-terminal-amidated thanatin against clinical isolates of extended-spectrum β-lactamase-producing *Escherichia coli*. *J. Infect. Dis. 203*, 273−282.

(12) Wu, G., Li, X., Fan, X., Wu, H., Wang, S., Shen, Z., and Xi, T. (2011) The activity of antimicrobial peptide S-thanatin is independent on multidrug-resistant spectrum of bacteria. *Peptides 32*, 1139−1145.

(13) Matsuzaki, K., Sugishita, K., Harada, M., Fujii, N., and Miyajima, K. (1997) Interactions of an antimicrobial peptide, magainin 2, with outer and inner membranes of Gram-negative bacteria. *Biochim. Biophys. Acta 1327*, 119−130.

(14) Matsuzaki, K. (1999) Why and how are peptide-lipid interactions utilized for self-defense? Magainins and tachyplesins as archetypes. *Biochim. Biophys. Acta 1462*, 1−10.

(15) Shai, Y. (2002) Mode of action of membrane active antimicrobial peptides. *Biopolymers 66*, 236−248.

(16) Fehlbaum, P., Bulet, P., Chernysh, S., Briand, J. P., Roussel, J. P., Letellier, L., Hetru, C., and Hoffmann, J. A. (1996) Structure-activity analysis of thanatin, a 21-residue inducible insect defense peptide with sequence homology to frog skin antimicrobial peptides. *Proc. Natl. Acad. Sci. U.S.A. 93*, 1221−1225.

(17) Mandard, N., Sodano, P., Labbe, H., Bonmatin, J. M., Bulet, P., Hetru, C., Ptak, M., and Vovelle, F. (1998) Solution structure of thanatin, a potent bactericidal and fungicidal insect peptide, determined from proton two-dimensional nuclear magnetic resonance data. *Eur. J. Biochem. 256*, 404−410.

(18) Boutin, J. M., Richer, J., Tremblay, M., Bissonette, V., and Voyer, N. (2007) Synthesis and characterization of peptide nanostructures chemisorbed on gold. *New J. Chem. 31*, 741−747.

(19) Zhang, Y. P., Lewis, R., Hodges, R. S., and McElhaney, R. N. (1992) Interaction of a peptide model of a hydrophobic transmembrane α-helical segment of a membrane protein with phosphatidylcholine bilayers: Differential scanning calorimetric and FTIR spectroscopic studies. *Biochemistry 31*, 11579−11588.

(20) Savitzky, A., and Golay, M. J. E. (1964) Smoothing and differentiation of data by simplified least squares procedures. *Anal. Chem. 36*, 1627−1639.

(21) Rance, M., and Byrd, R. A. (1983) Obtaining high-fidelity spin-1/2 powder spectra in anisotropic media: Phase-cycled Hahn echo spectroscopy. *J. Magn. Reson. 52*, 221−240.

(22) Bennett, A. E., Rienstra, C. M., Auger, M., Lakshmi, K. V., and Griffin, R. G. (1995) Heteronuclear decoupling in rotating solids. *J. Chem. Phys. 103*, 6951−6958.

(23) Kim, J. G., and Kim, J. D. (1991) Vesicle to micelle transitions of egg phosphatidylcholine liposomes induced by nonionic surfactants, poly(oxyethylene) cethyl esters. *J. Biochem. 110*, 436−442.

(24) Epand, R. M., and Epand, R. F. (2003) Liposomes as models for antimicrobial peptides. *Methods Enzymol. 372*, 124−133.

(25) Karop, G. (2010) The structure and function of the plasma membrane. In *Cell and Molecular Biology: Concepts and Experiments*, 6th ed., pp 117−172, John Wiley & Sons, Inc., Hoboken, NJ.

(26) Epand, R. M., and Epand, R. F. (2011) Bacterial membrane lipids in the action of antimicrobial agents. *J. Pept. Sci. 17*, 298−305.

(27) Seelig, J. (1978) ^{31}P nuclear magnetic resonance and the head group structure of phospholipids in membranes. *Biochim. Biophys. Acta 515*, 105−140.

(28) Seelig, J., and Seelig, A. (1980) Lipid conformation in model membranes and biological membranes. *Q. Rev. Biophys. 13*, 19−61.

(29) Speyer, J. B., Sripada, P. K., Dasgupta, S. K., Shipley, G. G., and Griffin, R. G. (1987) Magnetic orientation of sphingomyelin lecithin bilayers. *Biophys. J. 51*, 687−691.

(30) Asher, I. M., and Levin, I. W. (1977) Effects of temperature and molecular interactions on vibrational IR spectra of phospholipid bilayers. *Biochim. Biophys. Acta 468*, 63−72.

(31) Casal, H. L., Cameron, D. G., Smith, I. C. P., and Mantsch, H. H. (1980) *Acholeplasma-laidlawii* membranes: Fourier-transform

DOI: 10.1021/acs.biochem.5b00442
Biochemistry XXXX, XXX, XXX−XXX

infrared study of the influence of protein on lipid organization and dynamics. *Biochemistry 19*, 444−451.
(32) Kodati, V. R., and Lafleur, M. (1993) Comparison between orientational and conformational orders in fluid lipid bilayers. *Biophys. J. 64*, 163−170.
(33) Lee, M. K., Cha, L., Lee, S. H., and Hahm, K. S. (2002) Role of amino acid residues within the disulfide loop of thanatin, a potent antibiotic peptide. *J. Biochem. Mol. Biol. 35*, 291−296.
(34) Wu, G., Fan, X., Li, L., Wang, H., Ding, J., Hongbin, W., Zhao, R., Gou, L., Shen, Z., and Xi, T. (2010) Interaction of antimicrobial peptide S-thanatin with lipopolysaccharide in vitro and in an experimental mouse model of septic shock caused by a multidrug-resistant clinical isolate of *Escherichia coli*. *Int. J. Antimicrob. Agents 35*, 250−254.
(35) Wu, G., Wu, H., Li, L., Fan, X., Ding, J., Li, X., Xi, T., and Shen, Z. (2010) Membrane aggregation and perturbation induced by antimicrobial peptide of S-thanatin. *Biochem. Biophys. Res. Commun. 395*, 31−35.
(36) Barth, A. (2007) Infrared spectroscopy of proteins. *Biochim. Biophys. Acta 1767*, 1073−1101.
(37) Krimm, S. (1962) Infrared spectra and chain conformation of proteins. *J. Mol. Biol. 4*, 528−540.
(38) Krimm, S., and Bandekar, J. (1986) Vibrational spectroscopy and conformation of peptides, polypeptides, and proteins. *Adv. Protein Chem. 38*, 181−364.
(39) Surewicz, W. K., Mantsch, H. H., and Chapman, D. (1993) Determination of protein secondary structure by Fourier transform infrared spectroscopy: A critical assessment. *Biochemistry 32*, 389−394.
(40) Goormaghtigh, E., Cabiaux, V., and Ruysschaert, J.-M. (1994) Determination of soluble and membrane protein structure by Fourier transform spectroscopy. II. Experimental aspects, side-chain structure and H/D exchange. In *Physico-chemical methods in the study of biomembranes* (Hilderson, H. J., and Ralston, G. B., Eds.) pp 363−403, Plenum Press, New York.
(41) Wu, L., McElheny, D., Takekiyo, T., and Keiderling, T. A. (2010) Geometry and efficacy of cross-strand Trp/Trp, Trp/Tyr, and Tyr/Tyr aromatic interaction in a β-hairpin peptide. *Biochemistry 49*, 4705−4714.
(42) Xu, Y., Du, D., and Oyola, R. (2011) Infrared study of the stability and folding kinetics of a series of β-hairpin peptides with a common NPDG turn. *J. Phys. Chem. B 115*, 15332−15338.
(43) Wu, L., McElheny, D., Setnicka, V., Hilario, J., and Keiderling, T. A. (2012) Role of different β-turns in β-hairpin conformation and stability studied by optical spectroscopy. *Proteins 80*, 44−60.
(44) Chirgadze, Y. N., Fedorov, O. V., and Trushina, N. P. (1975) Estimation of amino-acid residue side-chain absorption infrared spectra of protein solutions in heavy-water. *Biopolymers 14*, 679−694.
(45) Braiman, M. S., Briercheck, D. M., and Kriger, K. M. (1999) Modeling vibrational spectra of amino acid side chains in proteins: Effects of protonation state, counterion, and solvent on arginine C-N stretch frequencies. *J. Phys. Chem. B 103*, 4744−4750.
(46) Lewandowska, A., Oldziej, S., Liwo, A., and Scheraga, H. A. (2010) Mechanism of formation of the C-terminal β-hairpin of the B3 domain of the immunoglobulin binding protein G from *Streptococcus*. III. Dynamics of long-range hydrophobic interactions. *Proteins 78*, 723−737.
(47) Jas, G. S., Hegefeld, W. A., Middaugh, C. R., Johnson, C. K., and Kuczera, K. (2014) Detailed microscopic unfolding pathways of an α-helix and a β-hairpin: Direct observation and molecular dynamics. *J. Phys. Chem. B 118*, 7233−7246.
(48) Raussens, V., Ruysschaert, J. M., and Goormaghtigh, E. (2003) Protein concentration is not an absolute prerequisite for the determination of secondary structure from circular dichroism spectra: A new scaling method. *Anal. Biochem. 319*, 114−121.
(49) Kwon, M. Y., Hong, S. Y., and Lee, K. H. (1998) Structure-activity analysis of brevinin 1E amide, an antimicrobial peptide from *Rana esculenta*. *Biochim. Biophys. Acta 1387*, 239−248.

DOI: 10.1021/acs.biochem.5b00442
Biochemistry XXXX, XXX, XXX−XXX